Electrochemical and Solid-State Letters, **4** (4) C26-C29 (2001)
1099-0062/2001/4(4)/C26/4/$7.00 © The Electrochemical Society, Inc.

Superconformal Electrodeposition of Copper

T. P. Moffat,[a,*,z] D. Wheeler,[a] W. H. Huber,[b] and D. Josell[a]

[a]Materials Science and Engineering Laboratory and [b]Electrical and Electronic Engineering Laboratory, National Institute of Standards and Technology, Gaithersburg, Maryland 20899, USA

A model of superconformal electrodeposition is presented based on a local growth velocity that is proportional to coverage of a catalytic species at the metal/electrolyte interface. The catalyst accumulates at the interface through reaction with the electrolyte. More importantly, if the concentration of the catalyst precursor in the electrolyte is dilute, then surface coverage within small features can change far more rapidly due to changing interface area. In such a case, the catalyst effectively floats on the interface during deposition, with changes in coverage coupled to alterations in arc-length of the moving surface. The local coverage therefore increases during conformal growth on a concave surface, resulting in a corresponding increase in the local deposition rate. The opposite is true for a convex surface. The model is supported by experiments and simulations of superconformal copper deposition in 350-100 nm wide features. The model also has significant implications for understanding the influence of adsorbates on the evolution of surface roughness during electrodeposition.
 [DOI: 10.1149/1.1354496]

Manuscript submitted December 14, 2000, revised manuscript received January 3, 2001. Available electronically February 26, 2001.

Recent demonstration and adaptation of superconformal copper electrodeposition in the damascene process for microelectronic fabrication represents a significant advance enabling a new generation of integrated circuits. Such ''superfilling'' of trenches and vias results from more rapid growth at the bottom of the trenches than at the sidewalls. Early modeling studies focused on leveling theory, where the location-dependent growth rate derived from diffusion-limited accumulation of an inhibiting species.[1-3] However, it was necessary to empirically modify the theory to capture the experimentally observed shape evolution.[1,2] Although the derived constitutive equations provide a reasonable description of feature filling, the required modification challenges the physical veracity of the model.

Subsequent research revealed that superconformal deposition in submicrometer features involves competitive interaction between species that accelerate and inhibit deposition.[4-7] In addition, a model system was identified that exhibits the characteristics required for successful on-chip metallization.[7] The electrolyte is a combination of three additives; chloride (Cl), polyethylene glycol (PEG), and 3-mercapto-1-propanesulfonate (MPSA). In this electrolyte, inhibition is provided by the interaction between PEG-Cl and the copper surface while acceleration is associated with competitive adsorption of MPSA or some derivative thereof. The competitive interaction results in hysteresis of current-voltage (i-η) polarization curves as well as the ''overfill'' phenomena.[7] The latter term describes the situation where the originally concave surface profile associated with growth in the trench becomes convex due to sustained acceleration of the local deposition rate. Such overfill cannot be rationalized by the transport-limited inhibition model outlined above.[4-7]

This paper presents a model of superconformal deposition in which the kinetics and mechanism of the metal deposition reaction are dependent on the fractional surface coverage θ of a catalytic or accelerating species (derived here from MPSA). At a smooth planar electrode, accumulation scales with C_{MPSA} which is in the μmol/L range. In the first approximation, the adsorbed species remains on the copper-electrolyte interface during copper deposition without being incorporated into the solid. The coverage θ saturates at a monolayer. In contrast, on nonplanar geometries, such as rough or patterned surfaces, local θ also changes inversely to changes of local electrode surface area during growth. Accordingly, the coverage increases during conformal growth on a concave surface while the opposite is true for a convex surface. This process gives rise to superconformal deposition. For this to occur in a given submicrometer feature, the changing coverage of the active surface species caused by surface compression or dilation must outweigh changes due to accumulation from the electrolyte or loss from incorporation in the growing solid. Surface diffusion of the catalytic species is assumed to be negligible during deposition.

The Deposition Reaction: Obtaining Kinetic Parameters

The capacity for the MPSA-derived adsorbates to simultaneously float on the growing surface and accelerate the rate of copper deposition was explored using slow scan rate voltammetry. Deposition on freshly polished polycrystalline copper electrodes was examined in acidified cupric sulfate solutions containing 88 μmol/L PEG, 1 mmol/L Cl, and a range of C_{MPSA}. Additional details are published elsewhere.[7] The i-η curves are displaced toward positive potentials as C_{MPSA} increases from 0 to 15.90 μmol/L (Fig. 1), thus MPSA accelerates deposition. The slope of the curve increases with C_{MPSA}, indicating that the rate-determining step of the copper deposition reaction changes, likely from cuprous ion generation to consumption.[8-10] At high overpotentials the deposition rate is independent of potential due to transport limitations on the cupric ion.

The i-η curves may be described by the Butler-Volmer equation including cupric ion depletion at high overpotentials[11]

$$i = i_{\mathrm{o}}\left(1 - \frac{i}{i_{\mathrm{L}}}\right)\exp\left(-\frac{\alpha F}{RT}\eta\right) \qquad [1]$$

The overpotential, η, defines the deviation from equilibrium, the exchange current density, i_{o}, describes the dynamic exchange that characterizes equilibrium, the transport-limited deposition rate, i_{L} is

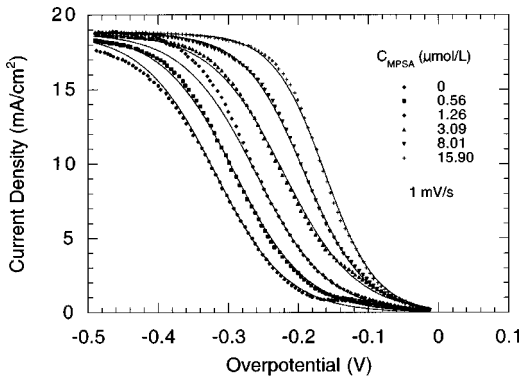

Figure 1. Voltammetric curves showing acceleration of copper deposition as a function of C_{MPSA}. Lines are calculated; dots are experimental data. Sweep rates 1 mV/s.

* Electrochemical Society Active Member.
z E-mail: tmoffat@nist.gov

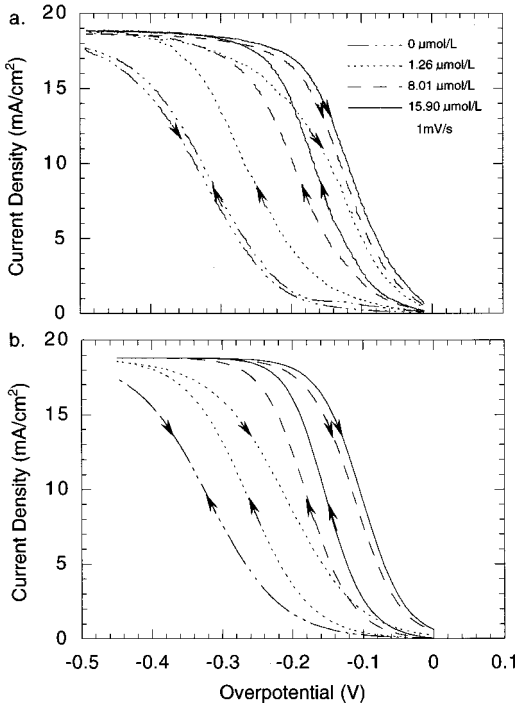

Figure 2. (a) Slow sweep CVs revealing hysteresis as a function of C_{MPSA}. (b) Simulations of the i-η curves according to Eq. 2 adsorption and accumulation of a MPSA-derived catalyst. Sweep rates 1 mV/s.

determined by boundary layer diffusion and free convection, the transfer coefficient, α, defines the slope of the curve, and F is Faraday's constant.

Cyclic i-η curves (Fig. 2a) reveal hysteresis that arises from accumulation of an MPSA derivative on the surface. The acceleration on the reverse sweep saturates at $C_{MPSA} \geq 15.90\ \mu$mol/L (Fig. 2a), indicating saturation of the surface coverage. Time-dependent fractional surface coverage $\theta(t)$ was calculated for each electrolyte by assuming irreversible statistical adsorption.[12,13] The rate constant for this process, k_{eff}, may reflect the limitations of the interfacial reaction or, alternatively, may correspond to a mass transport constraint across a boundary layer δ. Considering transport parameters for MPSA identical to those for Cu^{2+} and saturation coverage Γ_o corresponding to a $\sqrt{3}\times\sqrt{3}$ R30° structure on Cu(111), and estimate of $k_{eff} = D/\Gamma_o\delta = 4.01 \times 10^2$ L/mol·s

$$\theta(t) = 1 - \exp(-C_{MPSA}k_{eff}t) \quad [2]$$

Fitting Eq. 1 to the resulting $i(\theta)$-$\eta(\theta)$ curves to estimate $i_o(\theta)$ and $\alpha(\theta)$ was simplified by fitting only the points when $i = 10$ mA/cm^2, chosen for experimental sensitivity (Fig. 1). The corresponding θ increases with C_{MPSA} of the electrolyte, defining $i_o(\theta)$ and $\alpha(\theta)$ over the full range θ:[0,1]. The simulated i-η curves in Fig. 2b were obtained using Eq. 1 and 2 with $i_o(\theta)$ and $\alpha(\theta)$ as estimated. The hysteresis evident in Fig. 2b is in agreement with the experiments (Fig. 2a), particularly for higher C_{MPSA}.

Feature Filling: Modeling and Experiment

Simulations were performed to explore the effect of compression (dilation) of the floating species during filling of submicrometer features using $i(\theta,\eta)$ obtained above. Linearized $i_o(\theta)$ and $\alpha(\theta)$ (to simplify the calculations) still capture the general features of the experimental i-η curve, giving the local interface current density (from Eq. 1)

$$i(\theta) = (0.4726\,\theta + 0.0374)\exp\left(-\frac{(0.5 + 0.25\,\theta)F}{RT}\eta\right) \quad [3]$$

where the local velocity (*i.e.*, current density) of the interface is given by $\mathbf{u} = v\mathbf{n}$, with $v = i(\theta)\Omega/2F$ (2 for Cu^{2+}/Cu, with atomic volume Ω) and $\mathbf{n}$ the normal pointing into the liquid. The fractional change of θ with time t is determined by change in local area, *i.e.*, the instantaneous front velocity v times the local curvature of the interface κ (positive for concave)

$$\frac{d\theta}{dt} = \frac{i\Omega}{2F}\kappa\,\theta \quad [4]$$

As the interface moves, the local coverage increases on the concave surface and decreases on the convex portions. Analysis demonstrates that this area change leads to far greater changes in surface coverage within ''superfilling'' features than that provided by the electrolyte. It is therefore a reasonable approximation to replace the time-dependent accumulation by an initial surface coverage θ_i equal to the estimated MPSA derived species that accumulates from the electrolyte in the first ~20 s of potentiostatic deposition (when most filling of the trenches occurs). Overpotentials η were chosen to allow direct comparison with filling experiments.

Numerical evaluation.—To solve this problem, a set of nodes was enumerated sequentially along the interface. The jth node has position $\mathbf{r}_j$ and, for visualization, is connected to the $j-1$ and $j+1$ nodes by segments. An explicit scheme in time is used such that the position of the jth node after a time step is given by

$$\mathbf{r}_j = \mathbf{r}_j^o + \mathbf{u}^o\Delta t \quad [5]$$

where the superscript o represents the value prior to the time step. The time step Δt is given by

$$\Delta t = \frac{1}{10}\min\left(\frac{d_j}{v_j}, \frac{d_{j-1}}{v_j}\right) \quad [6]$$

for all j, where $d_j = |\mathbf{r}_{j+1} - \mathbf{r}_j|$. This choice of time step prevents overlapping of the interface. In terms of the x and y coordinates of the nodes, the local normal $\mathbf{n}$ pointing into the electrolyte is

$$\mathbf{n} = \left(\frac{y_{j-1} - y_{j+1}}{|r_{j+1} - r_{j-1}|}, \frac{x_{j+1} - x_{j-1}}{|r_{j+1} - r_{j-1}|}\right) \quad [7]$$

for enumeration of the nodes along the interface such that the electrolyte would be to the left of a person walking along the direction of increasing j. The coverage of the jth node is determined from

$$\theta_j = \frac{\theta_j^o(d_j^o + d_{j-1}^o)}{d_j + d_{j-1}} \quad [8]$$

This formulation conserves solute locally as required. At times it is also necessary to change the topology by adding and deleting nodes to maintain the interface integrity. A topology change is initiated when $d_j > 2\Delta x$ (nodes too far apart) or $|\mathbf{r}_m - \mathbf{r}_n| < 0.9|m - n|\,\Delta x$, with $|m - n| < 4$ (nodes too close together), where Δx is the initially uniform node spacing. If a new node m is added, it is placed midway between node j and $j+1$, thus

$$\mathbf{r}_m = (\mathbf{r}_{j+1} + \mathbf{r}_j)/2 \quad [9]$$

with local conservation of solute ensured by giving the new node a value

$$\theta_j = (\theta_{j+1} + \theta_j)/2 \quad [10]$$

When deleting a node j, local conservation of catalyst is ensured as follows. Using linear interpolation, conservation of catalyst is ensured by updating nodes $j-1$ and $j+1$ as follows

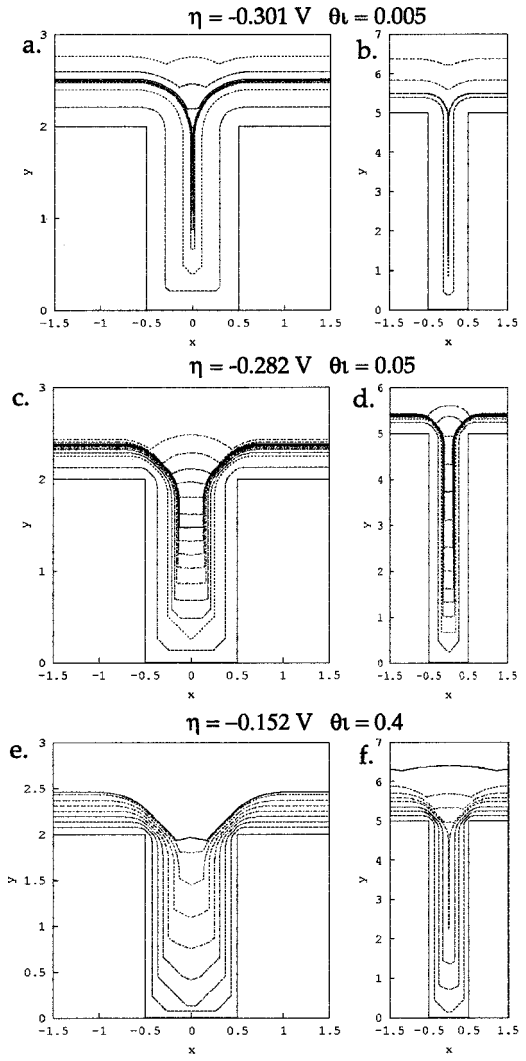

Figure 3. Simulations of copper deposition in two trench geometries, aspect ratios 1.5 and 5, for C_{MPSA}: 0.5, 5.0, and 40.0 μmol/L (top to bottom).

$$\theta_{j-1}(d_{j-2} + d_{j-1}) + \theta_j(d_{j-1} + d_j) + \theta_{j+1}(d_j + d_{j+1}) = \theta_{j-1}{}^N(d_{j-2} + |r_{j+1} - r_{j-1}|) + \theta_{j+1}{}^N(d_{j+1} + |r_{j+1} - r_{j-1}|) \quad [11]$$

where the superscript *N* indicates the new value. A second equation for the two unknowns is obtained from imposing equal gradients of θ tangent to the interface before and after node elimination

$$\frac{(\theta_{j+1}{}^N - \theta_{j-1}{}^N)}{|r_{j+1} - r_{j-1}|} = \beta \frac{(\theta_{j+1} - \theta_{j-1})}{|r_{j+1} - r_{j-1}|} \quad [12]$$

To impose equal composition gradients before and after node elimination, β should equal unity. However, for a physically reasonable solution, the θ^N values must be positive as well as have positive coefficients of proportionality to the θ values. To ensure these conditions are met, β is given by

$$\beta = \min\left(1, \frac{(d_{j-2} + d_{j-1})(d_{j-1} + d_j)}{|r_{j+1} - r_{j-1}|(d_{j-2} + |r_{j+1} - r_{j-1}|)}, \frac{(d_j + d_{j+1})(d_{j-1} + d_j)}{|r_{j+1} - r_{j-1}|(d_{j+1} + |r_{j+1} - r_{j-1}|)}\right) \quad [13]$$

All nodes are effectively resequenced after the time step and the process begins again.

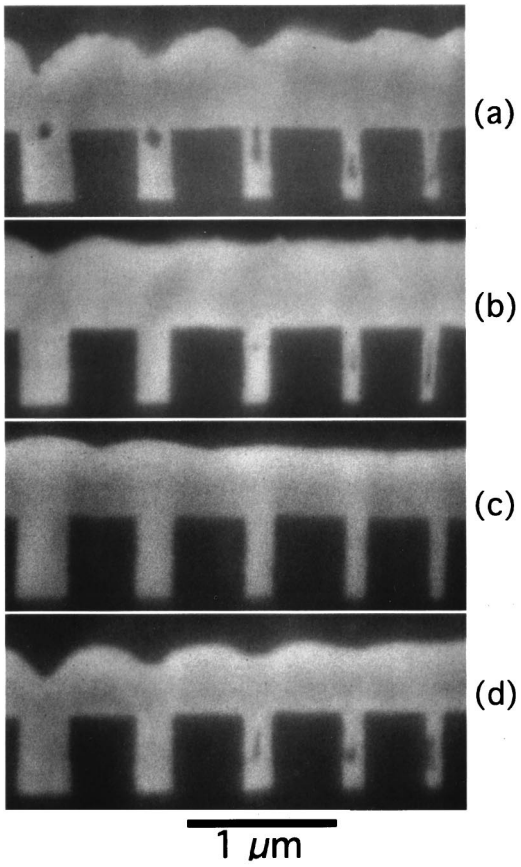

Figure 4. SEMs of trenches filled from electrolytes with C_{MPSA}: 0, 0.5, 5, and 40 μM/L (top to bottom).

The algorithm recognizes that a seam is forming by the number of nodes being deleted. Appropriate for such an event, instead of implementing Eq. 11 and 12 to ensure conservation of solute, the values θ at the adjacent nodes are not updated, and the adsorbed catalyst is lost (trapped).

Modeling results.—The simulations yield varying behavior depending on the aspect ratio (trench height/width) for 330 and 100 nm wide, 0.5 μm deep, trenches, initial coverage and overpotential (Fig. 3). ''Superfilling'', as shown in Fig. 3a, c, d, and e, is achieved when the catalytic surface species becomes sufficiently concentrated in the bottom of the trenches that bottom-up filling occurs. As the growth front approaches the top of the trench an inversion of the growth front curvature occurs forming the bumps visible above the trenches. The bottom-up growth is most dramatic with the optimal conditions (Fig. 3c and d). In this case, θ at the bottom steadily increases, resulting in rapidly accelerating upward growth with minimal sidewall motion. Consistent with observations, these simulations show that the bottom-up filling process has an incubation period of conformal growth as the concentration of the catalytic species on the concave trench corners begins to increase. In contrast, if the aspect ratio of the trenches is too great, or the differential velocity along the surface profile is too small, the sidewalls impinge before the bottom of the trench can escape. A vertical seam then forms in the center of the trench as shown in Fig. 3b and f. Thus, smooth continuous surface profiles characterize ''superfilling''; cusps denote marginal, incomplete fill, or seam formation. Although this first generation model does not consider depletion of cupric ion within the trench, the transition between seam formation and ''superfilling'' is expected to correlate directly with void and void-free filling, respectively.

Comparison of modeling and experiment.—Predictions of the

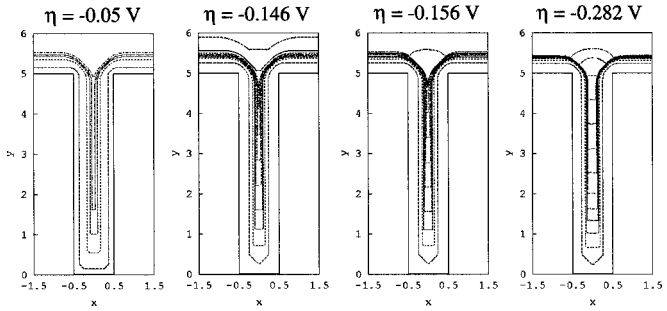

Figure 5. Simulations of the impact of overpotential on superfilling of trenches with an aspect ratio of 5, for $\theta_i = 0.05$ (corresponding to $C_{MPSA} \approx 5$ μmol/L).

model concerning the effect of trench dimensions and additive concentration C_{MPSA}, with interfacial kinetics fully constrained by the i-η measurements, were compared with filling experiments. Copper was electroplated in patterned trenches under different deposition conditions. The trench widths varied from 350 to 100 nm with the aspect ratio ranging from 1.5 to 5.0. The specimens were deposited under potentiostatic conditions with the deposition potential corresponding to a steady-state current density ~10 mA/cm^2 for the given electrolyte. Further experimental details may be found elsewhere.[7] Deposition from an additive-free cupric sulfate solution yields voids in all trenches along with the cusped surface profile anticipated for conformal deposition (Fig. 4a). For $C_{MPSA} = 0.5$ μmol/L voids are apparent for trenches with an aspect ratio greater than 2 (Fig. 4b). This agrees with the corresponding simulations (Fig. 3a) where superfilling is barely accomplished at an aspect ratio of 2 with seam formation evident at higher aspect ratios (Fig. 3b). For $C_{MPSA} = 5$ μmol/L distinct superfilling behavior is evident; all trenches are filled with small bumps above them (Fig. 4c). The simulations shown in Fig. 3c,d are completely congruent with these observations. For $C_{MPSA} = 40$ μmol/L voids appear in trenches 200 nm and smaller. The grooved surface profile indicates that the system has reverted toward a conformal growth mode. Again, this agrees with the corresponding simulations where a transition from superfilling to seam formation occurs between an aspect ratio of 2 and 5 (Fig. 3e and f).

The dependence of trench filling on C_{MPSA} is understood within the model. In dilute solutions ($C_{MPSA} \approx 0.5$ μmol/L), coverage θ is so low that the geometrically driven enrichment yields insufficient acceleration for the bottom-up filling. In concentrated solution, the opposite applies; the initial surface coverage is so high that saturation is approached and the spatial variation in deposition rate is too small for superfilling. For $C_{MPSA} \approx 5$ μmol/L near-optimum initial coverage enables superfilling in all the trenches examined.

The impact of applied potential η on superfilling was also assessed by simulation. The effect of varying voltage is evident in Fig. 5 where, for given θ_i, a transition from seam formation to superfilling is predicted to occur at ~0.150 V. Under appropriate conditions, the θ dependent kinetics provided by the Cl-PEG-MPSA system might in fact be capable of filling aspect ratios as high as 10 (Fig. 6), although mass transport considerations will likely be significant for such geometries.[14]

The magnitude of the voltammetric hysteresis measured in Fig. 2a (maximized for a scan rate of 1 mV/s with C_{MPSA} between 1.26 and 3.01 μmol/L) is a direct reflection of the range over which the deposition rate can be altered by the adsorbing species. Thus, the combination of the surface catalyst mediated growth model and i-η hysteresis measurements may be used to develop electrolyte chemistries for superfilling application.

Finally, note an intriguing analogy between the modeled surface-area driven changes of absorbate coverage at a growing solid/liquid interface and the force balance experiments performed on Langmuir troughs used to study two-dimensional adsorbate phase transition at liquid surfaces.

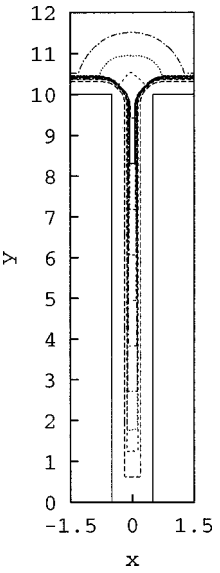

Figure 6. Simulations of superfilling a trench with an aspect ratio of 10, for $\eta = -0.282$ V and $\theta_i = 0.05$ (C_{MPSA}: 5 μmol/L).

Conclusions

In summary, a simple catalyst mediated deposition model has been shown to quantitatively predict three essential experimental observations relevant to superfilling submicrometer features in damascene processing, namely, accelerated growth from the bottom of the trench, inversion of the growth front and bump formation, and an incubation period prior to the onset of rapid bottom-up filling. From a broader perspective, it is important to note that this model inherently yields superconformal deposition as long as the surface coverage remains below saturation. This model has general implications for understanding the widespread use of organics additives to produce smooth ''bright'' surfaces by electrodeposition, and is clearly distinct from traditional leveling models, which are based on diffusion limited accumulation of inhibiting molecules.

The National Institute of Standards and Technology assisted in meeting the publication costs of this article.

References

1. P. C. Andricacos, C. Uzoh, J. O. Dukovic, J. Horkans, and H. Deligianni, *IBM J. Res. Dev.*, **42**, 567 (1998).
2. H. Deligianni, J. O. Dukovic, P. C. Andricacos, and E. G. Walton, in *Electrochemical Processing in ULSI Fabrication and Semiconductor/Metal Deposition II*, P. C. Andricacos, P. C. Searson, C. Reidsma-Simpson, P. Allongue, J. L. Stickney, and G. M. Oleszek, Editors, PV 99-9, p. 52, The Electrochemical Society Proceedings Series, Pennington, NJ (2000).
3. A. C. West, *J. Electrochem. Soc.*, **147**, 227 (2000).
4. J. Reid and S. Mayer, in *Advanced Metallization Conference 1999*, M. E. Gross, T. Gessner, N. Kobayashi, and Y. Yasuda, Editors, p. 53, MRS, Warrendale, PA (2000).
5. T. Ritzdorf, D. Fulton, and L. Chen, in *Advanced Metallization Conference 1999*, M. E. Gross, T. Gessner, N. Kobayashi, and Y. Yasuda, Editors, p. 101, MRS, Warrendale, PA (2000).
6. E. Richard, I. Vervoort, S. H. Brongersma, H. Bender, G. Beyer, R. Palmans, S. Lagrange, and K. Maex, in *Advanced Metallization Conference 1999*, M. E. Gross, T. Gessner, N. Kobayashi, and Y. Yasuda, Editors, p. 149, MRS, Warrendale, PA (2000).
7. T. P. Moffat, J. E. Bonevich, W. H. Huber, A. Stanishevsky, D. R. Kelly, G. R. Stafford, and D. Josell, *J. Electrochem. Soc.*, **147**, 4524 (2000).
8. S. Krzewska, *Electrochim. Acta*, **42**, 3531 (1997) and references therein.
9. M. Yokoi, S. Konishi, and T. Hayashi, *Denki Kagaku oyobi Kogyo Butsuri Kagaku*, **51**, 311 (1983).
10. M. Yokoi, S. Konishi, and T. Hayashi, *Denki Kagaku oyobi Kogyo Butsuri Kagaku*, **52**, 218 (1984).
11. A. J. Bard and L. R. Faulkner, *Electrochemical Methods, Fundamental and Applications*, John Wiley & Sons, New York (1980).
12. O. Dannenberger, M. Buck, and M. Grunze, *J. Phys. Chem. B*, **103**, 2202 (1999).
13. L. S. Jung and C. T. Campbell, *Phys. Rev. Lett.*, **84**, 5164 (2000).
14. K. Takahashi and M. E. Gross, *J. Electrochem. Soc.*, **146**, 4499 (1999).